



4-2006


Stretch Increases Alveolar Epithelial Permeability to Uncharged Micromolecules

Kenneth Joseph Cavanaugh
University of Pennsylvania

Taylor Sitarik Cohen
University of Pennsylvania

Susan S. Margulies
University of Pennsylvania, margulies@seas.upenn.edu

Follow this and additional works at: http://repository.upenn.edu/be_papers

 Part of the [Biomedical Engineering and Bioengineering Commons](#), and the [Cellular and Molecular Physiology Commons](#)

Recommended Citation

Cavanaugh, K., Cohen, T., & Margulies, S. S. (2006). Stretch Increases Alveolar Epithelial Permeability to Uncharged Micromolecules. *American Journal of Physiology - Cell Physiology*, 290 (4), C1179-C1188. <http://dx.doi.org/10.1152/ajpcell.00355.2004>

This paper is posted at ScholarlyCommons. http://repository.upenn.edu/be_papers/214
For more information, please contact repository@pobox.upenn.edu.

Stretch Increases Alveolar Epithelial Permeability to Uncharged Micromolecules

Abstract

We measured stretch-induced changes in transepithelial permeability in vitro to uncharged tracers 1.5–5.5 Å in radius to identify a critical stretch threshold associated with failure of the alveolar epithelial transport barrier. Cultured alveolar epithelial cells were subjected to a uniform cyclic (0.25 Hz) biaxial 12, 25, or 37% change in surface area (ΔSA) for 1 h. Additional cells served as unstretched controls. Only 37% ΔSA (100% total lung capacity) produced a significant increase in transepithelial tracer permeability, with the largest increases for bigger tracers. Using the permeability data, we modeled the epithelial permeability in each group as a population of small pores punctuated by occasional large pores. After 37% ΔSA , increases in paracellular transport were correlated with increases in the radii of both pore populations. Inhibition of protein kinase C and tyrosine kinase activity during stretch did not affect the permeability of stretched cells. In contrast, chelating intracellular calcium and/or stabilizing F-actin during 37% ΔSA stretch reduced but did not eliminate the stretch-induced increase in paracellular permeability. These results provide the first in vitro evidence that large magnitudes of stretch increase paracellular transport of micromolecules across the alveolar epithelium, partially mediated by intracellular signaling pathways. Our monolayer data are supported by whole lung permeability results, which also show an increase in alveolar permeability at high inflation volumes (20 ml/kg) at the same rate for both healthy and septic lungs.

Keywords

ventilator-induced lung injury, acute lung injury, barrier properties

Disciplines

Biomedical Engineering and Bioengineering | Cellular and Molecular Physiology | Engineering

Stretch increases alveolar epithelial permeability to uncharged micromolecules

Kenneth J. Cavanaugh, Taylor S. Cohen, and Susan S. Margulies

Department of Bioengineering, University of Pennsylvania, Philadelphia, Pennsylvania

Abstract

We measured stretch-induced changes in transepithelial permeability in vitro to uncharged tracers 1.5–5.5 Å in radius to identify a critical stretch threshold associated with failure of the alveolar epithelial transport barrier. Cultured alveolar epithelial cells were subjected to a uniform cyclic (0.25 Hz) biaxial 12, 25, or 37% change in surface area (ΔSA) for 1 h. Additional cells served as unstretched controls. Only 37% ΔSA (100% total lung capacity) produced a significant increase in transepithelial tracer permeability, with the largest increases for bigger tracers. Using the permeability data, we modeled the epithelial permeability in each group as a population of small pores punctuated by occasional large pores. After 37% ΔSA , increases in paracellular transport were correlated with increases in the radii of both pore populations. Inhibition of protein kinase C and tyrosine kinase activity during stretch did not affect the permeability of stretched cells. In contrast, chelating intracellular calcium and/or stabilizing F-actin during 37% ΔSA stretch reduced but did not eliminate the stretch-induced increase in paracellular permeability. These results provide the first in vitro evidence that large magnitudes of stretch increase paracellular transport of micromolecules across the alveolar epithelium, partially mediated by intracellular signaling pathways. Our monolayer data are supported by whole lung permeability results, which also show an increase in alveolar permeability at high inflation volumes (20 ml/kg) at the same rate for both healthy and septic lungs.

Keywords

ventilator-induced lung injury; acute lung injury; barrier properties

VENTILATOR-INDUCED LUNG INJURY and mechanical ventilation of patients with acute respiratory distress syndrome (ARDS) are associated with increased paracellular permeability of the alveolar epithelium to large molecules (e.g., albumin) (18), as well as decreased alveolar surfactant activity, decreased lung compliance, and increased patient mortality (9,23). These ventilation-related health risks may be a result of excessive lung inflation, because animal and isolated lung studies demonstrate that noncyclic lung inflation at 100% total lung capacity increases pulmonary permeability (14–16,24) and that high inflation volumes can increase the permeability of the alveolar wall to water and radioactive macromolecular tracers (4,14–16, 24). Recent large-scale clinical trials concluded that low-volume mechanical ventilation reduces mortality in patients with acute or chronic lung damage (5,22) and suggested that minimizing lung inflation and the corresponding epithelial deformation may improve a patient's outcome. Controversy surrounding these conclusions (40) underscores the need for additional research to determine the mechanisms and thresholds of ventilator-induced lung injury.

Given that the epithelium lining the alveolar airspaces provides the primary barrier to solute and macromolecular transport in the healthy lung (30), it is reasonable to propose that excessive stretch associated with large lung inflations may impair alveolar epithelial barrier function directly and produce the increased paracellular permeability observed in these intact lung studies. Our group (6,7) has previously shown that high yet physiological magnitudes of applied cyclic stretch decrease intracellular alveolar epithelial tight junction protein content and increase the tight junction permeability to a fluorescent ouabain derivative 15–20 Å in radius. However, the paracellular permeability of the stretched alveolar epithelium has not yet been measured directly because it has proven difficult to culture the cells onto a substrate that is flexible, permeable, and biocompatible.

In this study, we extend our previous investigations and present the first direct measurements of the effect of stretch magnitude on paracellular permeability in the cultured alveolar epithelium. Using a novel method to obtain epithelial permeability in intact stretched monolayers, we found that high yet physiological cyclic stretch magnitudes increased the paracellular permeability of the cells to micromolecules of various sizes and altered the size and distribution of the hypothetical equivalent pores that we developed to model transport through the tight junction. In addition, we investigated mechanically stimulated signal transduction pathways (48) that may potentially contribute to the stretch-induced paracellular permeability alterations. Cells possess many mechanically stimulated signal transduction pathways (48). Some of these pathways may potentially contribute to the stretch-induced paracellular permeability alterations observed in whole lungs. For example, intracellular Ca^{2+} levels ($[\text{Ca}^{2+}]_i$) and the activity of protein kinase C (PKC) and tyrosine kinase (TK) all have been shown to increase after application of tension in many types of cells, including alveolar type II cells (27,29,47). Rising $[\text{Ca}^{2+}]_i$ levels and kinase activity correlate to an increase in monolayer or whole lung permeability (2,26,36,37).

As a component of the protein framework that gives the cell its shape, F-actin (the polymerized, fibrous form of actin) also is believed to be an important sensor of mechanical stress in many types of cells, including epithelia (11). Application of cyclic stretch alters F-actin distribution in alveolar epithelial cells (32), whereas disruption of F-actin perturbs tight junction structure and function (7,31). Combining these results suggests the hypothesis that F-actin reorganization may negatively affect paracellular barrier function in epithelial monolayers.

Our present studies showed that chelating intracellular calcium levels and stabilizing the actin cytoskeleton each diminished the stretch-induced permeability increase, whereas inhibition of TK or PKC did not significantly alter poststretch epithelial permeability. These results support previous qualitative *in vitro* and *ex vivo* data and suggest that high physiological stretch magnitudes may be unsafe for clinical mechanical ventilation.

As an additional study to confirm that our monolayer preparation adequately represents the lungs of ARDS patients, whole lung permeability data measured using a large (55 kDa) tracer were obtained from rats that had been subjected to double cecal ligation and puncture (2CLP), which has been shown previously to provoke ARDS-like changes in the lungs, including hypoxemia, tachypnea, capillary leak, and neutrophilic infiltration (45). These whole lung data qualitatively agree with our cell preparation results, and they demonstrate that permeability changes in the whole lung are dependent on both the applied inflation volume and the disease state of the lungs.

MATERIALS AND METHODS

Cell Culture Protocol

Alveolar type II cells were isolated from healthy male Sprague-Dawley rats (180–200 g) according to a modification of the method of Dobbs et al. (12). This protocol was approved by the University of Pennsylvania Institutional Animal Care and Use Committee and has been described previously (6). After isolation, cells were suspended in minimum essential medium (MEM) with Earle's salts and supplemented with 10% fetal bovine serum, 25 µg/ml gentamicin, and 0.25 µg/ml amphotericin B (Life Technologies).

For the transport studies, cells were seeded at a density of 1×10^6 cells/cm² onto corona discharge-treated 0.003-in.-thick Mediflex 390 copolyester membranes (Mylan Technologies, Burlington, VT) coated with fibronectin (10 µg/cm²; Boehringer Mannheim Biochemicals, Indianapolis, IN) and poly-L-lysine (0.5 µg/cm²; Sigma) mounted in custom-made wells. For Western analyses of PKC and TK activity, cells were seeded at a density of 1×10^6 cells/cm² onto fibronectin-coated (10 µg/cm²) flexible Silastic membranes (Specialty Manufacturing, Saginaw, MI) mounted in custom-made wells. Both sets of wells were cultured in MEM supplemented as above and replaced daily for 5 days, by which time the cells had formed a confluent monolayer and displayed a phenotype consistent with that observed for cultured type I cells (35). At this time, experimentation was performed according to the protocols described below.

Assessment of Alveolar Epithelial Passive Barrier Properties

Stretch protocol—Cells were washed with Ringer solution (in mM: 126.4 NaCl, 25 NaHCO₃, 15 HEPES, 5.55 glucose, 5.4 KCl, 1.8 CaCl₂, 0.81 MgSO₄, and 0.78 NaH₂PO₄, pH 7.4) and were subjected to one of three stretch protocols or used as unstretched controls, for a total of four groups. For these studies, four isolations were performed for the unstretched controls and for each stretch magnitude. From each isolation, six wells were stretched at each magnitude, for a total of 24 wells per group. Paracellular permeability was assessed using a different tracer for each of these six wells.

Wells were mounted onto a custom-built cell-stretching device capable of applying equibiaxial strain to the samples at a precise user-defined magnitude and frequency, as previously described (43). Cells were stretched cyclically at 0.25 Hz for 1 h at 12, 25, or 37% changes in surface area (ΔSA). These changes in surface area approximately correspond to strains experienced by the alveolar epithelium in vivo at 70, 90, and 100% total lung capacity, respectively (42). Unstretched cells were used as controls. The temperature of the stretch device was maintained at 37°C. None of the stretch protocols resulted in loss of monolayer confluence, as determined by calcein-AM staining after stretch. The amount of cell death resulting from application of these magnitudes and modes of stretch has been shown not to exceed 8.9% in similarly cultured cells (43) and did not exceed $7.0 \pm 1.3\%$ in the current preparation.

Permeability measurement—After stretch, the cells were washed twice with Ringer solution. Each well was then mounted into a horizontally oriented Ussing chamber (World Precision Instruments, Sarasota, FL) such that transport could only occur through the portion of the well covered by cells. The basal portion of the Ussing chamber was filled with Ringer solution, whereas the apical portion was filled with an identical amount of Ringer solution spiked with 10 mM of one of the six tracers used: methylamine, alanine, valine, alanine-alanine (Ala-Ala), alanine-alanine-alanine (Ala-Ala-Ala), or leucine-leucine (Leu-Leu; Table 1). Each of the oligopeptides used was composed entirely of biologically inactive dextrorotary enantiomers of the amino acids, thus eliminating the possibility of cellular processing of these

tracers. None of the tracers used adversely affected cell viability over the time course of the experiment, as determined by ethidium homodimer-1 exclusion (data not shown).

Basal samples were drawn at time points of 0, 30, 60, 90, and 120 min after mounting in the Ussing chamber. Mounting the flexible membranes in the Ussing chamber added less than 5 min to the total experimentation time. The basal fluid volume was replenished with fresh Ringer solution after each sample was taken. The tracer concentration in the drawn samples was measured by mixing the sample with sodium borate and fluorescamine (3) and measuring the resulting fluorescence. Fluorescence of the samples was measured using a Fluoroskan Ascent fluorimeter (Thermo Labsystems, Vantaa, Finland) and calibrated against standards.

A first-principles model of paracellular transport was used for this system (24,25), which assumes that tracer mass in this system is conserved and that tracer transport across the epithelium follows first-order Fickian diffusion. Transport for each tracer is described by:

$$\ln \left[\frac{C_{A0} - \left(1 + \frac{V_B}{V_A}\right) C_B(t)}{C_{A0} - \left(1 + \frac{V_B}{V_A}\right) C_{B0}} \right] = - \frac{\left(1 + \frac{V_B}{V_A}\right) PS}{V_B} (t - t_0) \quad (1)$$

where C_{A0} is apical tracer concentration at the beginning of the time period, C_{B0} is basal tracer concentration at the beginning of the time period, $C_B(t)$ is basal concentration at time t , P is paracellular permeability of the monolayer to a specific tracer (units are length/time), S is surface area over which transport occurs, t_0 is initial time, V_A is apical volume, and V_B is basal volume.

Therefore, diffusion over the 120-min period of interest was modeled as a piecewise continuous function, where C_{A0} and C_{B0} were corrected to account for tracer diffusion and sample removal. For each individual well, P was calculated using Eq. 1, resulting in four values of P over the 120-min poststretch or postcontrol period. Tracer permeability was not a function of the time period in which the sample was drawn, as determined by the Tukey test for significance (49). The values of P for the replicate wells were then averaged to give permeability values for each tracer as a result of the applied stretch regimen. For each tracer, significant differences in permeability between each stretched condition and the unstretched control group were determined using Dunnett's test for multiple comparisons to a control group (49). Statistical significance was defined as $P < 0.05$. In separate studies, we determined that tracer permeability was not a function of the direction of tracer flux and that the osmotic gradient imposed by the presence of the tracer did not significantly affect the tracer permeability measurements (data not shown).

To determine the contribution of the tight junction to paracellular permeability in the absence of stretch, we determined the permeability of one unstretched well to alanine and Ala-Ala-Ala after treatment for 1 h with 2 mM 2-deoxy-D-glucose and 10 μ M antimycin A in glucose-free Ringer solution ($n = 3$ wells/group). This treatment has been shown to reduce the expression of tight junction proteins and to increase cell-cell spacing in identically cultured cells (7). We also measured the permeability of cell-free membranes to alanine and Ala-Ala-Ala in unstretched membranes and samples stretched cyclically at 37% ΔSA ($n = 3$ wells/group). Stretching bare membranes did not significantly alter the permeability of either tracer tested.

The transepithelial resistance of the monolayers on copolyester after 5 days in culture averaged $1,530 \pm 120 \Omega \cdot \text{cm}^2$ ($n = 6$ wells), whereas the resistance of the bare polyester membrane was measured at $650 \pm 30 \Omega \cdot \text{cm}^2$ ($n = 6$ membranes). In addition, the tracer permeability of the bare membrane was 28–110 times greater than that of cell-covered membranes. These results

indicate the alveolar epithelium formed monolayers with tight junctions that were functionally consistent with other preparations (8) and that the membrane itself did not contribute a significant amount of resistance to paracellular tracer flux.

Calculation of equivalent pore radius—The calculated permeability values for all the tracers were used to develop a model of the equivalent pore radii of the epithelium as a function of applied stretch. Equivalent pore radii are considered as a theoretical construct for the overall permeability of the epithelium, with larger radii and/or more numerous radii representing a more permeable monolayer. The model employed was adapted from the work of Kim and Crandall (4,25), with three assumptions. First, because our tracers were all oligopeptides and small, it was reasonable to assume they could be considered spherical in shape. Second, we assumed that convective transport was negligible and that paracellular transport was primarily via diffusion through two types of cylindrical pores, one with a smaller radius (subscript S) and one with a larger radius (subscript L). Finally, although the presence of an unstirred boundary layer near the monolayer surface could affect the accuracy of our transport measurements, previous studies have demonstrated that the effects of this layer are small, so we neglected the contribution of this layer (24). Paracellular tracer transport can thus be represented as:

$$PS = D[(A_{PS}/dx) f(a/r_S) + (A_{PL}/dx) f(a/r_L)] \quad (2)$$

where D is the diffusion coefficient of the tracer in water, A_p is the total pore area of the membrane, dx is the length of the cylindrical pores, a is the tracer radius, r is the pore radius, and P and S are defined as in Eq. 1. The polynomial function $f(a/r)$ represents the steric hindrance imposed on molecular transport by the walls of the equivalent pores and is defined by Renkin as $f(a/r) = (1 - a/r^2)(1 - 2.10a/r + 2.09a/r^3 - 0.95a/r^5)$ (38). Diffusion coefficients for all tracers were obtained by averaging the coefficient values calculated using the Wilke-Chang and Hayduk-Laudie methods of diffusion coefficient estimation (21,46). Tracer radius was estimated from molecular models obtained from the Protein Data Bank. These models were viewed using the freely distributed macromolecular viewing program Rasmol (<http://www.umass.edu/microbio/rasmol/index2.htm>). In our monolayers, a value of 200 nm was used for dx , as this the reported maximum thickness of type I cells in rats (39).

For each stretch and control condition, r_L and r_S were calculated from the available data by averaging the individual values calculated for each tracer. In addition, A_{PL} and A_{PS} were calculated from these equations using $n_S = A_{PS}/\pi r_S^2$ and $n_L = A_{PL}/\pi r_L^2$, where n_S and n_L represent the number of small and large pores in the system, respectively.

Determination of Mechanisms Involved in Poststretch Permeability Increase

Stretch protocol—Wells were mounted onto the custom-built cell-stretching device described. Cells were bathed in warm Ringer solution, maintained at 37°C, and stretched cyclically (0.25 Hz) for 1 h at 37% ΔSA (42), with one of four chemical modulators. Two control groups were included in this study. Unstretched, untreated wells were used to establish paracellular permeability in the absence of stretch and for comparisons with stretched wells. The second control group consisted of stretched, untreated wells, which were used to examine the effects of chemical treatment on stretch-induced changes in permeability. The experimental and control groups each consisted of six wells from each of four isolations, for a total of 24 wells per group.

While one group of stretched cells was left untreated, the remaining cells were chemically treated to block one of the putative pathways involved in increasing paracellular permeability as a result of the applied stretch. To chelate intracellular Ca^{2+} , we treated cells with 50 μM

BAPTA-AM (Molecular Probes) for 90 min. To inhibit PKC, we treated cells with 30 μM H-7 (Sigma) for 180 min. To inhibit TK, we treated cells with 50 μM genistein (Sigma) for 120 min. To stabilize F-actin, we treated cells with 1 μM jasplakinolide (Molecular Probes) for 120 min. Cells also were stretched at 37% ΔSA (0.25 Hz) in the presence of both BAPTA-AM and jasplakinolide to determine whether the protective effects of these chemicals were additive. The effect of dose and duration of each of these treatments on cell viability was tested using ethidium homodimer-1 staining, and none of the chemicals produced a significant increase in cell death in unstretched monolayers (<0.5%). Cell treatment was begun before stretch and continued during the entire 1-h stretch protocol. Additional cells were left unstretched and untreated as controls. Immediately after stretch, the cells were washed twice with Ringer solution to remove excess reagent. Paracellular transport was then assessed.

Transport measurement and modeling—After stretch, wells were mounted in Ussing chambers and monolayer permeability was measured and modeled using the tracers and techniques described above. A two-way analysis of variance showed that the time period in which the sample was taken did not significantly affect the measured permeability in the samples (49), indicating that chemical treatment did not alter the measured permeability after being washed off.

Data analysis—For each tracer, significant differences in permeability between each stretched and treated group and the stretched, untreated group were determined by using Dunnett's test for multiple comparisons to a control group (49). The permeability of stretched cells treated with BAPTA-AM or jasplakinolide also were compared with those of unstretched, untreated cells by using Dunnett's test to determine whether treatment completely prevented the previously observed stretch-induced permeability increase. The tracer permeabilities of unstretched cells treated with BAPTA-AM or jasplakinolide were compared with those of unstretched, untreated cells by using Dunnett's test to check whether exposure to these chemicals affects permeability in the absence of stretch. Stretched cells treated with both BAPTA-AM and jasplakinolide were compared with stretched cells treated with only one of these treatments by using the Dunnett's test to determine whether there was a synergistic effect when both treatments were used. In each of these analyses, statistical significance was defined as $P < 0.05$.

Determination of PKC and TK Activity After Stretch

Western blot analysis—To determine whether PKC and TK were activated by stretch, we examined the intracellular concentrations of the amino acid residues phosphorylated by these two kinase systems in both the presence and absence of stretch. PKC phosphorylates serine and threonine (41), whereas TK phosphorylates tyrosine residues. For these experiments, four cell isolations were performed for each group, resulting in 28 wells in the experimental and control groups. After 5 days in culture, the cells were washed with dye-free Dulbecco's modified Eagle's medium (Life Technologies).

Cells were stretched cyclically for 1 h at 37% ΔSA (0.25 Hz) and 37°C or left unstretched to serve as controls. After the stretch period, cells from each group were homogenized and the total protein concentration was determined according to a modification of a previously employed protocol (7). Bovine serum albumin (BSA; 0.1%) was used as the blocking agent to minimize background staining. The polyvinylidene difluoride (PVDF) membranes were incubated overnight with primary antibodies against rabbit phosphoserine, mouse phosphothreonine, or mouse phosphotyrosine (Zymed, South San Francisco, CA), each diluted 1:1,500 in 0.1% BSA. After the membranes were washed, incubation proceeded for 1 h with horseradish peroxidase-conjugated donkey anti-mouse or anti-rabbit secondary antibody (Zymed; 1:500 dilution). The PVDF membranes were washed and developed using enhanced

chemiluminescence. Each film was digitized, and the band intensities were measured and normalized with respect to total cellular protein content. For each amino acid, the unstretched and stretched groups were then compared using Student's *t*-test for statistical significance (defined as $P < 0.05$).

Whole Lung Studies

Male Sprague-Dawley rats (250–350 g) were anesthetized using isoflurane, and fecal peritonitis was induced via 2CLP using an 18-gauge needle as previously described (44). After the procedure, animals were resuscitated with 40 ml/kg sterile saline. All animals were killed within 24 h of the procedure according to the previously described method, followed by cannulation of the trachea and pulmonary artery, perfusion of the lungs with saline to remove blood, and en bloc excision of the whole lungs. Whole lungs were also removed from control animals that had not been subjected to puncture or ligation (sham group).

The lungs were kept moist with saline, placed in a custom dish on a multiphoton microscope (Bio-Rad, Hercules, CA), and perfused with 1.5 ml 100% FITC-labeled albumin (55 kDa; Sigma) via the pulmonary artery. The lungs were ventilated once via the tracheal cannula with a positive end-expiratory pressure (PEEP) of 4 cmH₂O and a tidal volume of either 6 or 20 ml/kg, corresponding to 12 or 25% ΔSA , respectively (42), at a frequency of 0.25 Hz. At end expiration, a stack of thirty 0.5- μ m-thick micrographs ($\times 60$) was obtained through the thickness of a field of subpleural alveoli. Ventilation was continued for 30 min, at which time another stack of images was obtained. From each time point, a series of eight images that clearly showed the cross section of the alveoli were selected for analysis. Intensity of five randomly chosen alveoli (avoiding interstitial areas and blood vessels) was taken at each of the selected depths. An average intensity for each time point was computed by taking a weighted average against the size of the alveolus so that larger alveoli had more of an influence. To minimize the effect of inter-lung variations in background signal, all average intensities were normalized to the baseline (*time 0*) values. Using these normalized and averaged values, we performed statistical comparisons between the healthy and septic lungs and between the 6 and 20 ml/kg ventilation conditions by using a three-way ANOVA. Tukey tests were used to make comparisons across all fields.

RESULTS

Stretch-Induced Permeability Increase

On the basis of the Tukey analysis of tracer permeabilities as a function of time, the monolayer barrier properties did not degrade or improve during the 120-min period of permeability measurement (data not shown). These results demonstrate that the stretch-induced barrier dysfunction observed at 37% ΔSA is irreversible for at least 120 min after cessation of stretch and that barrier function does not improve or worsen over the course of the experiment. Although wells were mounted in the chamber within 5 min after the stretch period ended, we cannot exclude the possibility that transient changes in permeability occurred < 5 min poststretch.

One hour of cyclic mechanical stretch at 37% ΔSA was the only magnitude that resulted in a significant increase in paracellular permeability to any of the tracers studied (Fig. 1). Furthermore, at this magnitude, permeability to all tracers was significantly increased (200–2,300% of tracer permeabilities of unstretched cells). Cyclic stretch at 12 and 25% ΔSA did not significantly increase the permeability of any tracer examined, compared with unstretched values.

Depleting unstretched cells of ATP via treatment with 2-deoxy-D-glucose and antimycin A resulted in an alanine permeability of 340% of untreated unstretched control values and an Ala-Ala-Ala permeability of 4,800% of control values (Fig. 1). Although 37% Δ SA significantly increased permeability compared with unstretched monolayers, these values were just below those from ATP-depleted cells, which established that stretch nearly completely compromised the epithelial tight junction barrier. These results indicate that a lack of tight junction integrity is sufficient to cause an increase in paracellular permeability.

Equivalent Pore Radius vs. Stretch

The calculated equivalent small- and large-pore radii for unstretched cells were 4.28 and 43.4 Å, respectively (Table 2). The small pore type was dominant by far, representing 99.9986% of the total equivalent pore population and 99.85% of the pore area available for transport. The pore dimensions did not change appreciably for cells stretched at magnitudes below 37% Δ SA. In these small stretch groups, the pore radii varied from 4.20 to 4.34 Å and from 41.2 to 48.6 Å for the small and large pores, respectively.

In contrast, cyclic application of 37% Δ SA altered the pore characteristics dramatically (Table 2). The small- and large-pore radii increased by 214 and 147% to 9.14 and 62.9 nm, respectively. The numbers of each pore present also changed after application of this stretch protocol. The number of small pores decreased to 3.3×10^8 pores (7% of unstretched values), whereas the number of large pores increased to 626×10^3 pores (921% of unstretched values). In addition, small pore representation dropped to 99.81% of the total pore population and 91.8% of the available pore area. These results indicate that this type of stretch especially facilitates transport of large molecules by increasing the area available for large molecule transport.

Chemical Prevention of Stretch-Induced Permeability Changes

Treatment with either BAPTA-AM or jasplakinolide resulted in significantly lower paracellular permeability in cells stretched cyclically for 1 h at 37% Δ SA (Fig. 2) compared with stretched cells receiving no treatment. The salutatory effects of chemical treatment were significant for tracers larger than methylamine but were more pronounced for the three largest tracer groups.

Despite the decrease in permeability after stretched cells were separately treated with these two chemicals, paracellular permeability was still significantly higher than that of unstretched, untreated cells (Fig. 2). This was true for all tracers tested after separate BAPTA-AM and jasplakinolide treatment. Therefore, these stretched, treated cells possessed permeability characteristics in between those of unstretched, untreated cells and stretched, untreated cells.

Unstretched wells that were treated with either BAPTA-AM or jasplakinolide possessed tracer permeabilities not significantly different from those of unstretched, untreated cells. This finding demonstrates that these two chemicals do not affect the permeability of unstretched cells; their mechanism of action involves stretch-activated pathways.

Compared with stretched cells treated with a single treatment of either BAPTA-AM or jasplakinolide, treatment of stretched cells with both BAPTA-AM and jasplakinolide significantly reduced epithelial permeability to only methylamine (Fig. 2) compared with jasplakinolide-treated cells stretched at 37% Δ SA. For the remainder of the tracers, the action of $[Ca^{2+}]_i$ and the actin cytoskeleton on paracellular permeability do not appear to be independent and may be part of the same pathway.

Compared with stretched, untreated cells, chemical treatment with genistein or H-7 failed to prevent a permeability increase in cells stretched cyclically for 1 h at 37% Δ SA. Tracer

permeabilities of all six tracers in these stretched, treated groups were not significantly different from those of stretched, untreated cells.

Equivalent Pore Analysis of Treated Cells

The theoretical small- and large-pore radii in unstretched cells separately treated with BAPTA-AM were 4.19 and 49.2 Å, respectively, and in unstretched, jasplakinolide-treated cells and small stretch (<37% Δ SA) groups, they were 4.31 and 52.6 Å, respectively (Table 3). These values are similar to those of unstretched, untreated cells (4.28 and 43.4 Å, respectively; Table 2), indicating that chemical treatment has little effect on the pore sizes of the alveolar epithelium in the absence of stretch.

Cyclic 37% Δ SA stretch of untreated cells produced equivalent pore radii of 7.53 and 57.9 Å in our alveolar epithelial monolayers. This calculation is based on data from a separate control group of untreated, stretched cells from that described in Fig. 1 and Table 2, yet the calculated pore radii are similar in both groups (see Table 2). BAPTA-AM treatment resulted in radii of 7.01 and 50.2 Å after stretch, whereas jasplakinolide incubation resulted in poststretch pore radii of 7.40 and 46.3 Å. Although permeability to all tracers larger than methylamine was significantly reduced with these treatments, this corresponds with more pronounced changes in the size of the large-pore radius than in the small-pore radius. Furthermore, compared with that of stretched, untreated cells, the total pore area occupied by the larger pores decreased in these two stretched and chemically treated groups, decreasing from 5.41 to 2.89% in BAPTA-AM-treated cells and to 3.54% in jasplakinolide-treated cells.

Stretched cells treated with both BAPTA-AM and jasplakinolide possessed pore radii of 6.80 and 43.9 Å (Table 3). With treatment, this small-pore radius is still higher than that of unstretched, untreated cells, whereas the large-pore radius is closer in value to that of unstretched, untreated cells than to stretched, treated cells.

In genistein-treated cells compared with stretched, untreated cells, the poststretch small-pore radius decreased slightly to 7.31 Å, whereas the large-pore radius increased slightly to 59.6 Å. Both small- and large-pore radii increased in H-7-treated cells. In both groups, the change in pore size was <10% compared with that in stretched, untreated cells, and these treatments did not result in significant improvement in stretch-induced permeability measurements. In addition, the percentage of pore area represented by large pores in both genistein- and H7-treated cells was similar to that in stretched, untreated cells, only decreasing from 5.41 to 5.17% after BAPTA-AM treatment and to 5.33% in H-7-treated cells. Moreover, these small fractional changes in pore radii with genistein- and H-7-treated, stretched cells (compared with untreated, stretched cells) are similar to those observed in small stretch (<37% Δ SA) groups compared with unstretched, untreated cells, further confirming that small changes in pore radii and pore area are not likely to result in permeability changes for molecules in the 1.5- to 5-Å range.

Stretch-Induced PKC/TK Activity

Application of cyclic 37% Δ SA did not significantly affect the intracellular levels of phosphoserine, phosphothreonine, or phosphotyrosine (Fig. 3). The poststretch concentrations of all three amino acids did not vary by >10% of the corresponding unstretched values. These results provide evidence that PKC and TK are not activated by stretch in rat alveolar epithelial cells maintained in culture for 5 days and stretched cyclically at 37% Δ SA.

Whole Lung Studies

ANOVA showed that time ($P < 0.0001$), tidal volume ($P < 0.05$), and interactions between health (septic or sham) and tidal volume ($P < 0.05$), between time and tidal volume ($P < 0.05$), and among tidal volume, health, and time ($P < 0.05$) were significant effects (Fig. 4). Tukey

comparisons show that after 30 min of ventilation, only septic animals ventilated at 20 ml/kg had significantly increased alveolar intensity compared with animals at initial time points ($P < 0.05$). Intensity after 30 min in lungs ventilated at 20 ml/kg significantly differed between septic and sham groups, with septic lungs being more permeable ($P < 0.05$). These data show that alveolar barrier properties are vulnerable to tidal volume-dependent permeability changes and that the effect of tidal volume is exacerbated by disease.

DISCUSSION

Our unstretched *in vitro* monolayer preparation is consistent with the observations of other investigators that the alveolar epithelium possesses a high resistance to paracellular transport. First, we measured an average resistance of $1,530 \Omega\text{-cm}^2$ in the unstretched monolayers, consistent with previously reported values of $>1,000 \Omega\text{-cm}^2$, marking it as one of the least permeable tissues in the body (8). Second, the mean permeability of unstretched cells to alanine was 6.43×10^{-6} cm/s, and the permeability to Ala-Ala-Ala was 6.07×10^{-8} cm/s. These permeability values are 92 and 5,140 times less than the corresponding tracer permeabilities of the bare copolyester membrane without cells, indicating that the unstretched monolayer is very resistant to paracellular transport compared with the cell-free polyester substrate. Third, our permeability data gathered from unstretched cultured alveolar epithelia agree well with whole lung transport data obtained using similarly sized tracers (4), with none of the epithelial permeabilities differing from its corresponding whole lung permeability by $>200\%$. Given the obvious morphological and functional differences in monolayers vs. whole lungs and the different methods used to gather data, this agreement is remarkable and indicates that the cultured alveolar epithelium can be used as an idealized preparation to study the barrier properties of the whole lung.

Our data indicate that there is a stretch magnitude above 25% ΔSA at which cyclic stretch irreversibly and significantly decreases alveolar epithelial barrier properties. Furthermore, we found that this stretch magnitude has a greater effect on large molecule permeability than on the passage of smaller compounds, although all increased significantly. Paracellular permeability after 37% ΔSA was less than the permeability of unstretched cells after treatment with 2-deoxy-D-glucose and antimycin A, indicating that this stretch magnitude, although injurious, does not fully disrupt the tight junction or lead to the rapid paracellular tracer transport observed in bare polyester membranes.

This threshold stretch magnitude is the same level that we reported previously to disrupt tight junction structure and barrier function in similarly cultured cells (6,7), although barrier properties were assessed using a single larger tracer (radius = 15–20 Å). Tight junction properties in these two studies also were not affected by lower magnitudes of stretch, similar to what was observed in the current preparation. These results also are comparable to those obtained using *ex vivo* animal models (4,24).

Our *in vitro* model has several inherent limitations that confound extrapolation of our results to the *in vivo* setting. The experimental monolayer contains only type I-like pneumocytes; it does not contain the mixed cellular composition of the intact epithelium (e.g., fibroblasts, type I and type II epithelial cells) or a biofidelic extracellular matrix, and the interstitial milieu may not be identical to that of the whole lung. In particular, the lack of surfactant in our experimental model is not representative of the environment *in vivo*. In addition, this *in vitro* model lacks macrophages and other immunocytes, and thus it does not mimic the response of the immune system to cyclic stretch. Despite these differences, our *in vitro* model is useful in that it isolates stretch-induced changes in alveolar barrier properties in the absence of the confounding variables of other cell types and nonuniform stretch conditions. With our system, we apply

well-characterized strain fields only to alveolar epithelial cells, the cell type most responsible for barrier property maintenance under baseline conditions (30).

To gain further insight into the permeability data, we modeled paracellular transport across stretched and unstretched monolayers as diffusive mass transfer through two populations of pores (38). Whereas this modeling approach has been employed previously for both whole lungs and cultured alveolar epithelial cells (4,25,33), it has never been used before to examine the effects of stretch on cells *in vitro*. The model predicted that stretch at 37% ΔSA would increase the radii of both small and large pores and increase the number of large pores, suggesting how high magnitudes of stretch may facilitate paracellular transport of macromolecules *in vivo*.

It is interesting to note that although the number of large pores increased after exposure to 37% ΔSA , both the small pore and total pore populations decreased, along with the total pore area of all pores (Table 3), and that this relationship held for the two significant chemical treatments, BAPTA and jasplakinolide. Although this finding seems to conflict with the poststretch increase in tracer permeability, this response can be explained by noting that much of the cross-sectional area of the small pores (and, to a lesser extent, the large pores) of unstretched cells is excluded from tracer transport because of steric hindrance. Increasing the radius of these small pores increases the area available for transport relative to the amount of “dead space,” resulting in more efficient tracer transport overall. Thus the increase in the small and large radii of both pores after stretch as well as the increase in the number of large pores both contribute to the increase in flux of all tracers tested after application of 37% ΔSA .

To further characterize the pore characteristics of the cultured epithelium, we used the data contained in Table 2 to calculate the total pore area represented by large and small pores for each of the stretched and unstretched groups. These calculations demonstrate that the decrease in total small pore area after stretch is greater than the gain in total large pore area, indicating that the gain in large pore area may potentially be due to merging of small pores. However, given that the amount of large pore area gained is only ~4% of the amount of small pore area lost after stretch, most (at least 96%) of the lost small pore area does not contribute to the formation of large pores and is “closed” or somehow removed from the tight junctional space.

When the dual-pore model of epithelial permeability was employed for undamaged intact rat lungs (4), the two pore radii were 5 and 34 Å, values that compare favorably with our calculated pore radii of 4.3 and 43 Å for the unstretched epithelium *in vitro*. There also is agreement between the two studies that the large pore area is a small percentage of the total pore area for all pores, indicating that small pores are much more prevalent than large pores in both models. A single-pore model was used to examine the effects of static mechanical strain on *ex vivo* bullfrog and rabbit lungs (24), and those results agree qualitatively with the current study such that static inflations at only very high lung deformations resulted in a change in permeability and that large tracer permeabilities increased more than those of small tracers.

Our whole lung study results indicate qualitative similarities with our monolayer permeability data in that both preparations demonstrate resistance to tracer transport through the epithelium at lower stretch or volume magnitudes and decreased resistance at higher magnitudes. The magnitude of maximum stretch differs between the two systems (37% ΔSA for the monolayers, ~25% ΔSA for the whole lungs), which could explain why no significant increase is observed in healthy lungs inflated at large tidal volume. The overall ANOVA, however, does show tidal volume to be a significant effect ($P < 0.05$). The apparent similarities between the two data sets suggest that the *in vitro* model may be appropriate for permeability measurements in a precisely controlled mechanical environment.

At higher levels of stretch, sham lungs displayed significantly lower tracer intensity than septic lungs ($P < 0.05$). Over the 30-min stretch duration, sham lungs ventilated at either tidal volume (6 or 20 ml/kg) did not accumulate significant amounts of tracer in the alveolar spaces compared with initial values. However, 30 min of ventilation at large tidal volumes (20 ml/kg) did significantly increase tracer intensity in the alveolar spaces of septic lungs compared with initial values. We conclude that lung health affected the stretch sensitivity of the epithelial barrier properties. This finding is consistent with the clinical observation that patients with ARDS are more likely to be adversely affected by mechanical ventilation (19), thus further supporting the validity of our selected experimental model.

We hypothesized that four potential chemical pathways may modulate stretch-induced permeability changes: PKC and TK activity, intracellular Ca^{2+} , and F-actin. We observed that there was no significant increase in the phosphorylation of the three amino acids primarily acted on by PKC and TK, as determined by Western blot analysis. Thus it is not surprising that treating our alveolar epithelial cells with either the PKC inhibitor H-7 or the TK inhibitor genistein failed to significantly affect the stretch-induced permeability increase at 37% ΔSA . Chelating $[\text{Ca}^{2+}]_i$ with BAPTA-AM reduced the extent of stretch-induced barrier dysfunction at 37% ΔSA compared with stretched, untreated cells for all tracers except methylamine, the smallest tracer used, indicating that $[\text{Ca}^{2+}]_i$ levels may affect tracer permeability in a size-dependent manner. Because treatment of unstretched cells with BAPTA-AM did not significantly affect paracellular permeability, we attribute this partial reduction in permeability dysfunction to the specific inhibition of stretch-activated pathways. However, the poststretch permeability of BAPTA-AM-treated cells was still significantly higher than that of unstretched, untreated cells and unstretched, treated cells, and so BAPTA-AM failed to completely prevent a significant increase in permeability in the cells stretched at 37% ΔSA .

We also hypothesized that stabilizing the F-actin of the alveolar epithelium during stretch would ameliorate the stretch-induced permeability increase. Our laboratory (35) previously showed that cyclic stretch at 25% ΔSA alters actin organization in a similar cell preparation. In this study, we found that stabilizing intracellular F-actin with jasplakinolide decreased the extent of barrier dysfunction in alveolar epithelial cells stretched cyclically but did not eliminate it completely. Jasplakinolide stimulates F-actin nucleation, thus promoting F-actin polymerization. The observed limited decrease in permeability of stretched, treated cells compared with stretched, untreated cells was true for all tracers except for the smallest, methylamine. As with BAPTA-AM treatment to reduce the $[\text{Ca}^{2+}]_i$, treatment with jasplakinolide did not alter paracellular permeability in unstretched cells. Stretch still resulted in a significant permeability increase in treated cells, but treatment modulated the stretch-induced permeability increase.

Because the other tracers did not experience a significant decrease in permeability after exposure to both chemicals, and the simultaneous treatment was not additive or synergistic, we hypothesize that both BAPTA-AM and jasplakinolide were inhibiting the same stretch-sensitive pathway in these cells. Under this hypothesis, $[\text{Ca}^{2+}]_i$ and actin are two upstream components of a communal terminal mechanism responsible for increasing paracellular permeability after stretch. We are hopeful that future studies to identify this terminal mechanism will lead to the development of specific therapies to inhibit stretch-induced permeability increases.

These mechanistic studies are illustrative but also are inherently qualitative in nature, because many of these pathways are linked and cannot be considered independent. For example, PKC activity is partly mediated by $[\text{Ca}^{2+}]_i$ in most types of cells (1). TK activation also is thought to be an event upstream of PKC activation (28). Actin rearrangement due to phorbol ester stimulation has been shown to be PKC-dependent in lung epithelial cells (13), whereas

vanadate and hydrogen peroxide redistribute actin in kidney cells through a TK-dependent mechanism (10). Moreover, the four transduction pathways that we examined are not the only ones known to affect tight junction permeability in cultured cells. Our group (7) previously showed that disrupting intracellular ATP metabolism significantly altered tight junction structure in our cells. Other chemical messengers such as glucose, ethanol, and the G protein family are also known to affect tight junction structure and function in other cell types (17). The contribution of these other mechanisms to stretch-induced permeability changes may be addressed in future studies. Perhaps blocking some of these additional pathways can keep the paracellular permeability of stretched alveolar epithelial cells at unstretched levels.

It also is possible that the damage to the paracellular barrier is not entirely due to the action of mechanically stimulated signal transduction pathways. The stresses directly generated by stretching the alveolar epithelium may be large enough to cause mechanical failure at the weakest locations within the monolayer. A purely mechanical contribution to barrier dysfunction would help to explain why the chemical modulations used in the study did not completely prevent barrier dysfunction after stretch. Further experimentation with the use of cells in which the elasticity of the internal tensile fibers has been altered or the surface area of contact between adjacent cells has been modified could potentially address the contribution of the mechanical properties of the cells to stretch-induced permeability changes.

Although our results have provided new information regarding the effects of mechanical stretch on barrier function, these results are by no means exhaustive. There are a number of variables that still need to be examined in this system. First, cells were only stretched for 1 h before permeability assessment. Stretching cells for a longer period of time may show that the more subtle changes we observed at low stretch magnitudes become more pronounced as the duration of exposure to mechanical stimulation increases. In addition, whereas our cell culture studies were performed using small tracer sizes, common blood proteins such as albumin and immunoglobulins are $>25 \text{ \AA}$ in radius (34) and are more similar in size to the FITC-albumin tracer used in our whole lung study. Although data exist indicating that the transport of molecules $>30 \text{ \AA}$ in radius across the alveolar epithelium may occur via endocytosis or other active processes (33), the similarities between the monolayers and whole lung results support the extrapolation of our in vitro data to the in vivo milieu. The applicability of our monolayer data to the in vivo setting is further supported by our previous finding that stretch of cultured alveolar epithelial cells at 37% ΔSA increased the paracellular permeability of the monolayer to a ouabain derivative $\sim 20 \text{ \AA}$ in radius (6). Finally, we only employed tracers with a neutral net charge. Because many blood proteins are charged (1), and paracellular permeability often varies depending on the charge of the traversing molecule (20), the question of the effect of tracer charge on paracellular permeability remains open to investigation.

With this study, we have demonstrated for the first time that high magnitudes of applied cyclic stretch increase the paracellular permeability of cultured alveolar epithelial monolayers. The permeability increases occurred partly through calcium- and actin-dependent mechanisms, although other chemical pathways may be equally involved. This study is the first to specifically identify alveolar epithelial cells as contributors to stretch-induced barrier failure. In addition, a well-defined and homogenous application of strain was used to identify the strain magnitude associated with increases in alveolar permeability. All previous studies in this area have employed whole lungs, which possess many cell types and do not typically allow for the precise measurement of alveolar strain. The data from these experiments suggest that high-magnitude lung inflation by itself may cause or potentiate pulmonary edema and micromolecular flux into the alveolar space in vivo.

Acknowledgments

Present address of K. J. Cavanaugh: Mail Code HFZ-450, Office of Device Evaluation, US Food and Drug Administration, 9200 Corporate Blvd., Rockville, MD 20850.

GRANTS Funds for this research were provided by the Whitaker Foundation and National Heart, Lung, and Blood Institute Grant R01 HL-57204.

REFERENCES

1. Alberts, B.; Bray, D.; Johnson, A.; Lewis, J.; Raff, M.; Roberts, K.; Walter, P. *Essential Cell Biology: An Introduction to the Molecular Biology of the Cell*. Garland; New York: 1998.
2. Banes AJ, Tsuzaki M, Yamamoto J, Fischer T, Brigman B, Brown T, Miller L. Mechanoreception at the cellular level: the detection, interpretation, and diversity of responses to mechanical signals. *Biochem Cell Biol* 1995;73:349–365. [PubMed: 8703408]
3. Bantan-Polak T, Kassai M, Grant KB. A comparison of fluorescamine and naphthalene-2,3-dicarboxaldehyde fluorogenic reagents for microplate-based detection of amino acids. *Anal Biochem* 2001;297:128–136. [PubMed: 11673879]
4. Berg MM, Kim KJ, Lubman RL, Crandall ED. Hydrophilic solute transport across rat alveolar epithelium. *J Appl Physiol* 1989;66:2320–2327. [PubMed: 2745296]
5. Brower RG, Matthay MA, Morris A, Schoenfeld D, Thompson BT, Wheeler A. Ventilation with lower tidal volumes as compared with traditional tidal volumes for acute lung injury and the acute respiratory distress syndrome. *N Engl J Med* 2000;342:1301–1308. [PubMed: 10793162]
6. Cavanaugh KJ, Margulies SS. Measurement of stretch-induced loss of alveolar epithelial barrier integrity with a novel in vitro method. *Am J Physiol Cell Physiol* 2002;283:C1801–C1808. [PubMed: 12388082]
7. Cavanaugh KJ, Oswari J, Margulies SS. Role of stretch on tight junction structure in alveolar epithelial cells. *Am J Respir Cell Mol Biol* 2001;25:584–591. [PubMed: 11713100]
8. Cheek JM, Kim KJ, Crandall ED. Tight monolayers of rat alveolar epithelial cells: bioelectric properties and active sodium transport. *Am J Physiol Cell Physiol* 1989;256:C688–C693.
9. Clark JG, Milberg JA, Steinberg KP, Hudson LD. Elevated lavage levels of N-terminal peptide of type III procollagen are associated with increased fatality in adult respiratory distress syndrome. *Chest* 1994;105:126S–127S. [PubMed: 8131607]
10. Collares-Buzato CB, Jepson MA, Simmons NL, Hirst BH. Increased tyrosine phosphorylation causes redistribution of adherens junction and tight junction proteins and perturbs paracellular barrier function in MDCK epithelia. *Eur J Cell Biol* 1998;76:85–92. [PubMed: 9696347]
11. Dewey CF Jr. Effects of fluid flow on living vascular cells. *J Biomech Eng* 1984;106:31–35. [PubMed: 6539406]
12. Dobbs LG, Gonzalez R, Williams MC. An improved method for isolating type II cells in high yield and purity. *Am Rev Respir Dis* 1986;134:141–145. [PubMed: 3637065]
13. Dwyer-Nield LD, Miller AC, Neighbors BW, Dinsdale D, Malkinson AM. Cytoskeletal architecture in mouse lung epithelial cells is regulated by protein kinase C- α and calpain II. *Am J Physiol Lung Cell Mol Physiol* 1996;270:L526–L534.
14. Egan EA. Lung inflation, lung solute permeability, and alveolar edema. *J Appl Physiol* 1982;53:121–125. [PubMed: 6288636]
15. Egan EA. Response of alveolar epithelial solute permeability to changes in lung inflation. *J Appl Physiol* 1980;49:1032–1036. [PubMed: 7440291]
16. Egan EA, Nelson RM, Olver RE. Lung inflation and alveolar permeability to non-electrolytes in the adult sheep in vivo. *J Physiol* 1976;260:409–424. [PubMed: 978536]
17. Fanning, AS. Organization and regulation of the tight junction by the actin-myosin complex. In: Cereijido, M.; Anderson, JM., editors. *Tight Junctions*. 2nd ed.. CRC; Boca Raton, FL: 2001. p. 265-284.
18. Gorin AB, Stewart PA. Differential permeability of endothelial and epithelial barriers to albumin flux. *J Appl Physiol* 1979;47:1315–1324. [PubMed: 536303]

19. Haake R, Schlichtig R, Ulstad DR, Henschen RR. Barotrauma. Pathophysiology, risk factors, and prevention. *Chest* 1987;91:608–613. [PubMed: 3549176]
20. Hardison WG, Lowe PJ, Shanahan M. Effect of molecular charge on para- and transcellular access of horseradish peroxidase into rat bile. *Hepatology* 1989;9:866–871. [PubMed: 2714737]
21. Hayduk W, Laudie H. Prediction of diffusion coefficients for non-electrolytes in dilute aqueous solutions. *AIChE J* 1974;28:611–615.
22. Hickling KG, Henderson SJ, Jackson R. Low mortality associated with low volume pressure limited ventilation with permissive hypercapnia in severe adult respiratory distress syndrome. *Intensive Care Med* 1990;16:372–377. [PubMed: 2246418]
23. Honda Y, Takahashi H, Shijubo N, Kuroki Y, Akino T. Surfactant protein-A concentration in bronchoalveolar lavage fluids of patients with pulmonary alveolar proteinosis. *Chest* 1993;103:496–499. [PubMed: 8432143]
24. Kim KJ, Crandall ED. Effects of lung inflation on alveolar epithelial solute and water transport properties. *J Appl Physiol* 1982;52:1498–1505. [PubMed: 6980871]
25. Kim KJ, Crandall ED. Heteropore populations of bullfrog alveolar epithelium. *J Appl Physiol* 1983;54:140–146. [PubMed: 6600738]
26. Kitamura T, Brauneis U, Gatmaitan Z, Arias IM. Extracellular ATP, intracellular calcium and canalicular contraction in rat hepatocyte doublets. *Hepatology* 1991;14:640–647. [PubMed: 1916664]
27. Liu M, Qin Y, Liu J, Tanswell AK, Post M. Mechanical strain induces pp60src activation and translocation to cytoskeleton in fetal rat lung cells. *J Biol Chem* 1996;271:7066–7071. [PubMed: 8636139]
28. Liu M, Tanswell AK, Post M. Mechanical force-induced signal transduction in lung cells. *Am J Physiol Lung Cell Mol Physiol* 1999;277:L667–L683.
29. Liu M, Xu J, Liu J, Kraw ME, Tanswell AK, Post M. Mechanical strain-enhanced fetal lung cell proliferation is mediated by phospholipase C and D and protein kinase C. *Am J Physiol Lung Cell Mol Physiol* 1995;268:L729–L738.
30. Lubman, RL.; Kim, KJ.; Crandall, ED. Alveolar epithelial barrier properties. In: Crystal, RG.; West, JB., editors. *The Lung: Scientific Foundations*. 2nd ed.. Lippincott-Raven; Philadelphia, PA: 1997. p. 585-602.
31. Madara JL, Barenberg D, Carlson S. Effects of cytochalasin D on occluding junctions of intestinal absorptive cells: further evidence that the cytoskeleton may influence paracellular permeability and junctional charge selectivity. *J Cell Biol* 1986;102:2125–2136. [PubMed: 3711143]
32. Margulies, SS.; Oswari, J.; Matthay, MA.; Tschumperlin, DJ. Alveolar epithelial cytoskeleton and cell vulnerability to stretch. *Am Soc Mech Eng; Bioengineering Conference; New York*. 1999. p. 517-518.
33. Matsukawa Y, Lee VH, Crandall ED, Kim KJ. Size-dependent dextran transport across rat alveolar epithelial cell monolayers. *J Pharm Sci* 1997;86:305–309. [PubMed: 9050797]
34. Matsukawa Y, Yamahara H, Yamashita F, Lee VH, Crandall ED, Kim KJ. Rates of protein transport across rat alveolar epithelial cell monolayers. *J Drug Target* 2000;7:335–342. [PubMed: 10721795]
35. Oswari J, Matthay MA, Margulies SS. Keratinocyte growth factor reduces alveolar epithelial susceptibility to in vitro mechanical deformation. *Am J Physiol Lung Cell Mol Physiol* 2001;281:L1068–L1077. [PubMed: 11597897]
36. Parker JC. Inhibitors of myosin light chain kinase and phosphodiesterase reduce ventilator-induced lung injury. *J Appl Physiol* 2000;89:2241–2248. [PubMed: 11090574]
37. Parker JC, Ivey CL, Tucker A. Phosphotyrosine phosphatase and tyrosine kinase inhibition modulate airway pressure-induced lung injury. *J Appl Physiol* 1998;85:1753–1761. [PubMed: 9804578]
38. Renkin EM. Filtration, diffusion, and molecular sieving through porous cellulose membranes. *J Gen Physiol* 1954;38:225–243. [PubMed: 13211998]
39. Schneeberger, EE. Alveolar type I cells. In: Crystal, RG.; West, JB., editors. *The Lung: Scientific Foundations*. 2nd ed.. Lippincott-Raven; Philadelphia, PA: 1997. p. 535-542.
40. Steinbrook R. How best to ventilate? Trial design and patient safety in studies of the acute respiratory distress syndrome. *N Engl J Med* 2003;348:1393–1401. [PubMed: 12672870]

41. Swannie HC, Kaye SB. Protein kinase C inhibitors. *Curr Oncol Rep* 2002;4:37–46. [PubMed: 11734112]
42. Tschumperlin DJ, Margulies SS. Alveolar epithelial surface area-volume relationship in isolated rat lungs. *J Appl Physiol* 1999;86:2026–2033. [PubMed: 10368370]
43. Tschumperlin DJ, Margulies SS. Equibiaxial deformation-induced injury of alveolar epithelial cells in vitro. *Am J Physiol Lung Cell Mol Physiol* 1998;275:L1173–L1183.
44. Weiss YG, Bouwman A, Gehan B, Schears G, Raj N, Deutschman CS. Cecal ligation and double puncture impairs heat shock protein 70 (HSP-70) expression in the lungs of rats. *Shock* 2000;13:19–23. [PubMed: 10638664]
45. Weiss YG, Tazelaar J, Gehan BA, Bouwman A, Christofidou-Solomidou M, Yu QC, Raj N, Deutschman CS. Adenoviral vector transfection into the pulmonary epithelium after cecal ligation and puncture in rats. *Anesthesiology* 2001;95:974–982. [PubMed: 11605941]
46. Wilke CR, Chang P. Correlation of diffusion coefficients in dilute solutions. *AIChE J* 1955;1:264–270.
47. Wirtz HR, Dobbs LG. Calcium mobilization and exocytosis after one mechanical stretch of lung epithelial cells. *Science* 1990;250:1266–1269. [PubMed: 2173861]
48. Wirtz HR, Dobbs LG. The effects of mechanical forces on lung functions. *Respir Physiol* 2000;119:1–17. [PubMed: 10701703]
49. Zar, J. *Biostatistical Analysis*. Prentice Hall; Upper Saddle River, NJ: 1999.

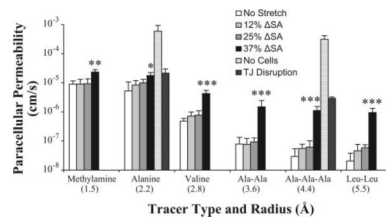
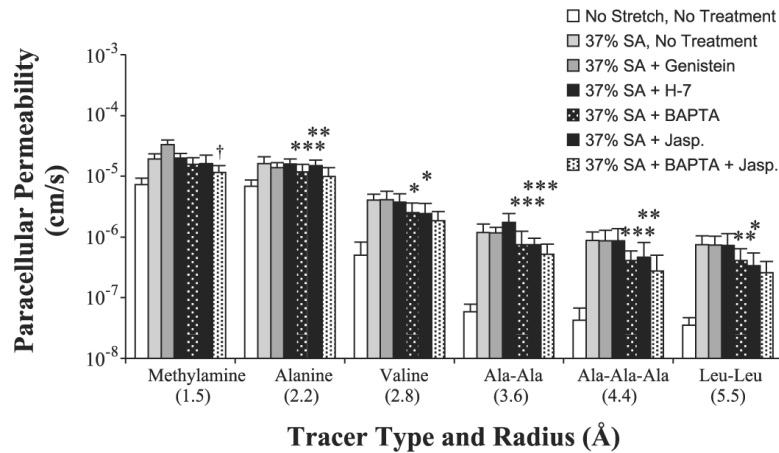


Fig. 1. Paracellular permeability vs. applied cyclic stretch. For cells stretched at a 37% change in surface area (ΔSA), tracer permeabilities significantly different from those of unstretched, untreated cells are indicated (* $P < 0.05$, ** $P < 0.005$, *** $P < 0.0001$). Note logarithmic scale for permeability. Data are presented as means (SD). Values in parentheses indicate tracer radius in Å. TJ, tight junction.

**Fig. 2.**

Tracer permeability at 37% Δ SA after chemical treatment. For stretched cells treated with either BAPTA-AM or jasplakinolide (Jasp), tracer permeabilities significantly different from those of stretched, untreated cells are indicated (* $P < 0.05$, ** $P < 0.01$, *** $P < 0.0001$). For stretched cells treated with both BAPTA-AM and jasplakinolide, tracer permeabilities significantly different from those of stretched cells treated with only jasplakinolide are indicated († $P < 0.05$). Note logarithmic scale for permeability. Data are presented as means (SD). Values in parentheses indicate tracer radius in Å.

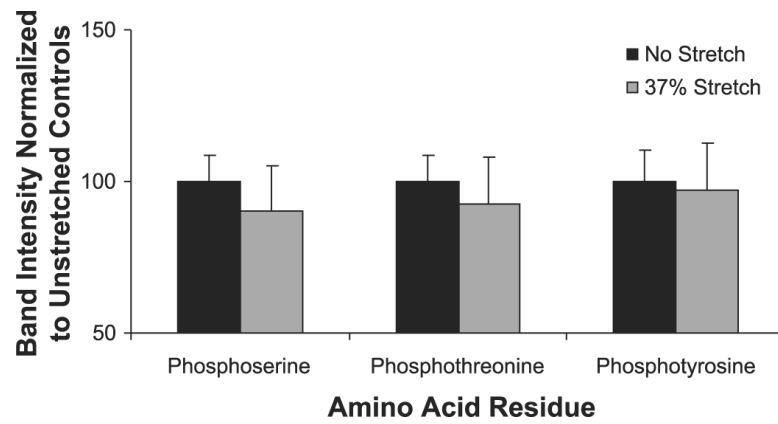


Fig. 3.

Phosphorylated amino acid residues before and after stretch. Increased phosphoserine and phosphothreonine residues are indicative of PKC activity, whereas elevated phosphotyrosine levels represent increased tyrosine kinase (TK) activity. Data are presented as mean (SD) band intensity normalized to that of corresponding unstretched controls.

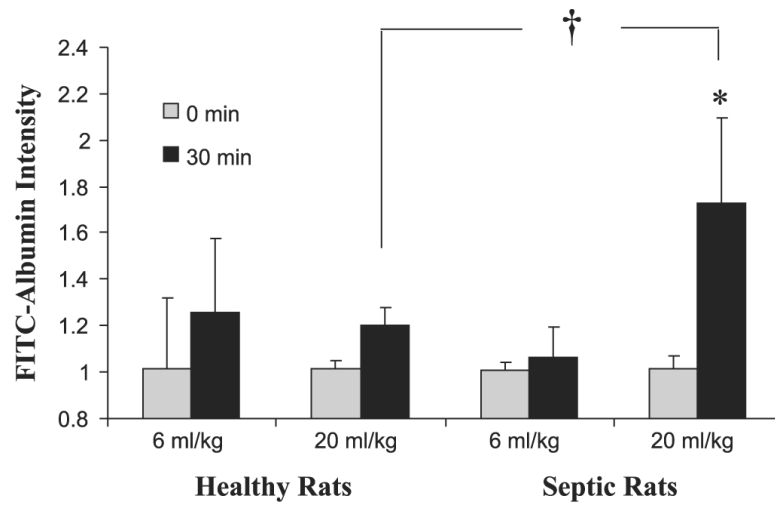


Fig. 4. Normalized FITC-albumin fluorescence intensity in whole rat lungs as a function of ventilation time, inflation volume, and rat health. Increased intensity is indicative of increased alveolar permeability. Data are presented as mean (SD) fluorescence intensity normalized to background signal ($n = 5$ alveoli per group). For permeabilities at 30 min, significant differences compared with baseline permeabilities are indicated ($*P < 0.01$). Significant differences between healthy and septic lungs are indicated ($\dagger P < 0.01$).

Table 1

Physical properties of tracers used

Tracer	$D, \text{cm}^2/\text{s} \times 10^{-6}$	Radius, Å
Methylamine	14.2	1.5
Alanine	8.95	2.2
Valine	7.14	2.8
Ala-Ala	6.22	3.6
Ala-Ala-Ala	4.97	4.4
Leu-Leu	4.45	5.5

D , diffusion coefficient of tracer in water.

Table 2

Equivalent pore characteristics of cyclically stretched cells

	No Stretch	12% Cyclic	25% Cyclic	37% Cyclic
Small-pore radius, Å	4.28	4.34	4.22	9.14
Number of small pores, $\times 10^7$	470	434	603	33
Small pore number compared with controls	100%	92%	128%	7%
Large-pore radius, Å	43	44	49	63
Number of large pores, $\times 10^3$	68	76	62	626
Large pore number compared with controls	100%	112%	92%	924%
Large pores per 10^6 total pores	14	17	10	1,886
Pore area occupied by large pores	0.15%	0.18%	0.14%	8.19%

Table 3

Equivalent pore characteristics of stretched and treated cells

	37% No Treatment	37% + BAPTA	37% + Genistein	37% + H-7	37% + Jasp.	37% + BAPTA/Jasp.
Small-pore radius, Å	7.53	7.01	7.31	7.65	7.4	6.8
Number of small pores, $\times 10^7$	62	64	68	57	52	56
Small pore number compared with 37% cyclic	100%	104%	109%	92%	84%	90%
Large-pore radius, Å	57.9	50.2	59.6	63.7	46.3	43.9
Number of large pores, $\times 10^3$	600	372	555	464	489	498
Large pore number compared with 37% cyclic	100%	62%	92%	77%	81%	83%
Large pores per 10^6 total pores	967	579	820	812	939	894
Pore area occupied by large pores	5.41%	2.89%	5.17%	5.33%	3.54%	3.59%

Jasp., jasplakinolide.